Hydrothermal synthesis and up-conversion luminescence of Ho^{3+}/Yb^{3+} co-doped CaF_2*

Yang Zheng(杨 征)[a], Guo Chong-Feng(郭崇峰)[a]†, Chen Ye-Qing(陈叶青)[b], Li Lin(李 琳)[a], Li Ting(李 婷)[a], and Jeong Jung-Hyun(郑仲铉)[b]‡

[a] National Key Laboratory of Photoelectric Technology and Functional Materials (Culture Base) in Shaanxi Province, Institute of Photonics & Photon-Technology, Northwest University, Xi'an 710069, China
[b] Department of Physics, Pukyong National University, Busan, 608-737, Korea

(Received 17 August 2013; revised manuscript received 1 November 2013; published online 10 April 2014)

CaF_2:Ho^{3+}/Yb^{3+} nano-particles with intense green up-conversion (UC) luminescence are successfully synthesized via a facile hydrothermal approach by using NH_4F as the fluoride source and Na_2EDTA as a chelating reagent. Powder X-ray diffraction (XRD), transmission electron microscopy (TEM), field emission scanning electron microscopy (FE-SEM), and UC emission spectra are used to characterize the structures, shapes, and luminescent properties of the samples. The effects from fluoride sources and chelating reagents on the formations of CaF_2 nano-particles are investigated, and the formation process is also deduced. Under the excitation of a 980-nm laser diode, the samples each show a green up-conversion emission centered at 540 nm corresponding to the $^5S_2/^5F_4 \rightarrow {}^5I_8$ transitions of Ho^{3+}. Moreover, the UC mechanisms of Ho^{3+}/Yb^{3+} co-doped CaF_2 nano-particles are also discussed.

Keywords: CaF_2, nano-particles, up-conversion, hydrothermal synthesis

PACS: 42.70.Km, 78.55.Hx **DOI:** 10.1088/1674-1056/23/6/064212

1. Introduction

In recent years, numerous efforts have been devoted to the investigation of rare-earth (RE) ions-doped up-conversion (UC) nano-particles (NPs) for their potential applications in displays,[1,2] optoelectronics,[3] biology and medicine,[4,5] and short wavelength lasers.[6] In particular, biological applications have aroused more research interest because UCNPs offer many advantages in comparison with the conventional organic dyes and semiconductor quantum dots down-conversion fluorescent materials, including high photostability, minimal photodamage to living organisms, deep light-penetration in tissues and long lifetimes of the involved RE energy levels.[7,8] Moreover, the UCNPs-based UC luminescence imaging is free of background auto-fluorescence, allowing high detection sensitivity.[9] Among the various RE-doped UCNPs, inorganic fluorides are the commonest hosts and have been investigated extensively due to their low energy phonons and efficient UC emissions.[10] For UC phosphors, because the phonon can give rise to nonradiative decay to suppress UC luminescence, it is necessary to choose a host with a much lower phonon energy in order to overcome the nonradiative decay and increase the UC efficiency. Up to now, $NaYF_4$ with its hexagonal structure and low phonon energy (360 cm^{-1}) is still regarded as the most efficient UC host.[11,12] Unfortunately, applications of $NaYF_4$ are restricted due to their inferior stabilities. As a member of fluorides, CaF_2 provides more excellent stability, a much wider transmission range, and lower phonon energy (328 cm^{-1}).[13–15] Therefore, CaF_2-based UC phosphor is expected to have a higher UC luminescence efficiency.

Rare earth ions-doped CaF_2 UC nano-particles with different shapes and sizes have been investigated extensively, such as green emitting monodisperse CaF_2:Yb^{3+}/Er^{3+} nanocrystals.[16] However, there has been little reported information about $Yb^{3+}Ho^{3+}$co-doped CaF_2 to date. Regarding Ho^{3+} ions, as another popular activator candidate for UC, several UC mechanisms have been proposed for Ho^{3+}-doped materials because the energy-levels of Ho^{3+} allow multiple excited state absorption (ESA) and/or energy transfer (ET) transitions from $^5I_7$, $^5I_6$, and $^5I_5$ levels to $^5S_2/^5F_4$ and even higher energy levels, which could activate an emission with a wide spectrum.[17] According to the previously published literature, the UC luminescence property is usually affected by the host structure, morphologies, and sizes of phosphor particles.[18,19] In order to improve the UC efficiency, it is important to control the sizes and morphologies of phosphor particles. In the present paper, we pay attention to the effects of reaction conditions including the chelating reagents and the fluoride sources on the morphology, particle size and UC luminescence of Yb^{3+}/Ho^{3+} co-doped CaF_2. In addition, the

*Project supported by the National Natural Science Foundation of China (Grant No. 11274251), the Natural Science Foundation of Hubei Province, China (Grant No. 2010CDB01607), the Technology Foundation for Selected Overseas Chinese Scholar, Ministry of Personnel of China (excellent), the Foundation of Shaanxi Educational Committee, China (Grant No. 11JK0528), and the Foundation of Key Laboratory of Photoelectric Technology in Shaanxi Province, China (Grant No. 12JS094).

†Corresponding author. E-mail: guocf@nwu.edu.cn
‡Corresponding author. E-mail: jhjeong@pknu.ac.kr

© 2014 Chinese Physical Society and IOP Publishing Ltd

effects of Ho^{3+} and Yb^{3+} concentrations on the photoluminescence of CaF_2:Ho^{3+}/Yb^{3+} are investigated. The growth mechanism of CaF_2:Ho^{3+}/Yb^{3+} nano-particles and UC mechanism are also discussed in detail.

2. Experiment

2.1. Synthesis

Ho^{3+} and Yb^{3+} co-doped CaF_2 nano-particles were prepared by the hydrothermal method. Stoichiometric quantities of raw materials, analytical grade $Ca(NO_3)_2{\cdot}4H_2O$, HNO_3, $C_{10}H_{14}N_2Na_2O_8{\cdot}2H_2O$ (Na_2EDTA), citric acid ($C_6H_8O_7{\cdot}H_2O$), NH_4F, $NaBF_4$, and high purity (99.99%) Ho_2O_3 and Yb_2O_3 were weighted. All chemical reagents were used directly without further purification. In a typical procedure, $Ho(NO_3)_3$ and $Yb(NO_3)_3$ solution was first prepared by dissolving corresponding oxides in a small amount of HNO_3 and then diluting with distilled water. Following that, $Ca(NO_3)_2{\cdot}4H_2O$ chelating agent Na_2EDTA or citric acid each with a certain amount was dissolved in the above aqueous solution under vigorous stirring for 0.5 h to obtain solution *A*. Second, the fluoride sources NH_4F or $NaBF_4$ were added into the above obtained solution *A* to form a translucent ivory solution. Next, the ivory solution was transferred into a 50-mL Teflon-lined autoclave. The autoclave was sealed and maintained at 160 °C for 24 h, then cooled down to room temperature naturally. The emulsion mixture product was centrifuged at 8000 rpm for 30 min, which caused sedimentation of the nano-particles and allowed the removal of the mother liquor. The precipitates were then washed and centrifuged several times with distilled water and absolute ethanol in turn, then dried at 60 °C for 6 h and crushed in an agate mortar to obtain samples.

2.2. Characterization

The powder X-ray diffraction (XRD) measurements were carried out in the range of $20^\circ \leq 2\theta \leq 60^\circ$ using a Rigaku–Dmax 3C powder diffractometer with Cu–Kα ($\lambda = 1.5406$ Å) radiation. The morphologies of the samples were examined by an FEI TF-20 transmission electron microscope (TEM) at an accelerating voltage of 200 kV and a field-emission scanning electron microscope (FESEM) (FE-SEM: JEOL JSM-6700F). The UC luminescence properties of the samples were examined by a Hitachi F-7000 fluorescence spectrophotometer with an external power-controllable 980-nm continuous semiconductor laser diode as the excitation source. All of the measurements were performed at room temperature.

3. Results and discussion

3.1. Structure and morphology

The phase compositions and crystal structures of the samples are identified by X-ray powder diffraction analysis. Figure 1 shows the results of the structure analysis and the TEM morphology of samples prepared with NH_4F and Na_2EDTA. Figures 1(a)–1(c) show the XRD patterns of phosphors CaF_2:0.5-mol%Ho^{3+}/5-mol%Yb^{3+} prepared with different fluoride sources and different chelating reagents by the hydrothermal method at 160 °C for 24 h. All detectable diffraction peaks are in agreement with those of the standard cubic CaF_2 (JCPDS card No. 89-4794) with lattice constant $a = 5.462$ Å, and no peaks from the impurity phase are detected. In the range of our experiments, the XRD patterns of all samples are similar, which indicates that doping of rare earth ions Ho^{3+} and Yb^{3+} does not cause any significant changes in the host structure. Here, we propose that Ho^{3+} and Yb^{3+} ions are expected to occupy the Ca^{2+} sites in the CaF_2 host, which will result in a decrease of the lattice parameter of the sample because the ionic radius of Ca^{2+} (1.12 Å for CN = 8) is larger than those of Ho^{3+} (1.015 Å for CN = 8) and Yb^{3+} (0.985 Å for CN = 8).[20] The calculated lattice parameter for *a* is 5.436 Å, which matches well with our deduction.

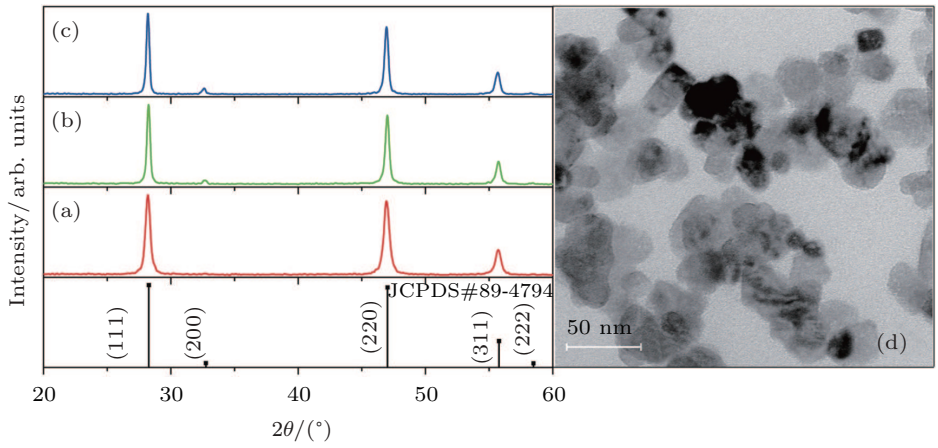


Fig. 1. (color online) XRD patterns of CaF_2:0.5-mol%Ho^{3+}/5-mol%Yb^{3+} samples prepared with different fluoride sources and different chelating reagents: (a) NH_4F and Na_2EDTA; (b) $NaBF_4$ and Na_2EDTA; (c) $NaBF_4$ and citric acid; and (d) TEM image of nano-particles prepared with NH_4F and Na_2EDTA.

Figure 1(d) shows the TEM image of UC nano-particles prepared with NH_4F and Na_2EDTA, in which we can observe cubic nano-particles with diameters ranging from 20 nm to 50 nm. According to the corresponding XRD pattern (Fig. 1(a)), the average size of nano-particles (D) could also be evaluated by using the Debye–Scherrer formula,[21] $D_{hkl} = K\lambda/(\beta\cos\theta)$, in which λ is the X-ray wavelength (1.5406 Å), β is the full width at half-maximum, θ is the diffraction angle, K is a constant (0.89), and D_{hkl} is the size along the (h k l) direction. Here, we use diffraction data at (111) 28.2°, (220) 46.9°, and (311) 55.7° to calculate the average particle size, which gives an estimated average size of 23.7 nm and is in good agreement with the result of TEM.

In our system, the morphologies and particle sizes of CaF_2 particles are adjusted by changing the chelating reagent and the fluoride source. It is worth pointing out that the concentration of the doping ions (Ho^{3+}/Yb^{3+}) in the CaF_2 host does not change the phase structure nor morphology nor size of the CaF_2 product in our system. The morphologies of samples were investigated by scanning electron microscopy (SEM). Figures 2(a)–2(c) show the SEM images of the samples prepared using different fluoride sources and chelating reagents. Figure 2(a) shows the morphology of CaF_2 particles in the presence of Na_2EDTA and NH_4F. It is found that uniform CaF_2 nano-particles with slight agglomeration are obtained. Obviously, the cubic nano-particles are side by side with each other. As is well known, the formation about a particle includes the initial production, subsequent growth, and final stabilization of nuclei, and the morphology and size of particles are mainly determined by the nucleation rate.[22,23] At first, in an aqueous solution, the Ca^{2+} chelate compounds are formed and the free Ca^{2+} ions concentration would decrease in solution. Then, with the increase of the reaction time and temperature, chelation of the Ca^{2+} chelate complexes would be weakened and Ca^{2+} ions would be released gradually. Therefore, the nucleation and growth of CaF_2 would undergo a long process, which would be conducive to the forming of uniform crystals. The probable reaction processes for forming CaF_2 in this condition can be summarized as follows:

$$C_{10}H_{14}N_2Na_2O_8 \rightarrow 2Na^+ + EDTA^{2-}, \quad (1)$$

$$Ca^{2+} + EDTA^{2-} \rightarrow Ca-EDTA(complex), \quad (2)$$

$$Ca-EDTA + 2F^- \rightarrow CaF_2 + EDTA^{2-}. \quad (3)$$

Except for the effect of Na_2EDTA, the fluoride source NH_4F also plays a key role in the controlled synthesis of CaF_2. For comparison with Fig. 2(a), the SEM image of the CaF_2 prepared with $NaBF_4$ serving as the F^- source in the presence of Na_2EDTA with the same parameters is displayed in Fig. 2(b), in which the irregular particles with diameters ranging from 50 nm to 150 nm are formed under this condition. When $NaBF_4$ serves as the fluoride supplier, the resulting morphology is quite different from using NH_4F as the fluoride source. $NaBF_4$ is slowly hydrolyzed to produce Na^+ cations, BO_3^{3-} and F^- anions as shown in the following equation:

$$BF_4^- + 3H_2O \rightarrow 3HF + F^- + H_3BO_3. \quad (4)$$

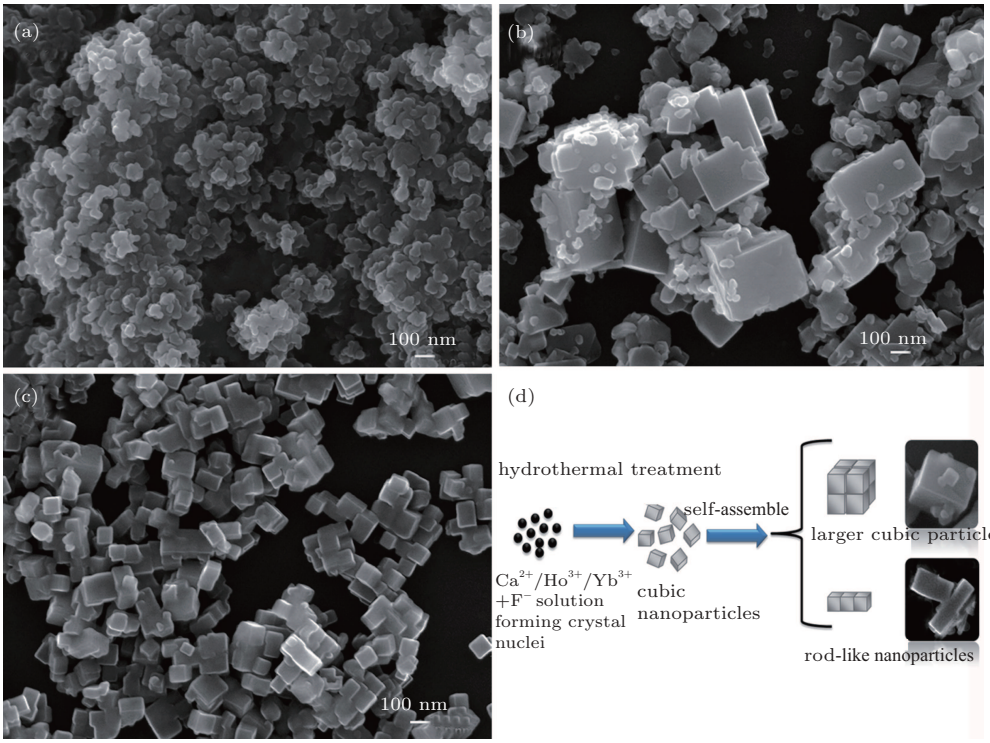


Fig. 2. (color online) SEM images of CaF_2:0.5-mol%Ho^{3+}/5-mol%Yb^{3+} samples prepared with different fluoride sources and different chelating reagents: (a) NH_4F and Na_2EDTA; (b) $NaBF_4$ and Na_2EDTA; (c) $NaBF_4$ and citric acid; and (d) schematic illustration of the formation and shape evolution of CaF_2:Ho^{3+}/Yb^{3+} particles.

It is noted that the added $NaBF_4$ has obvious effects on the morphology and particle size. Thus we can speculate that NH_4F and $NaBF_4$ are the key factors influencing the morphologies of the products, and the cations NH_4^+, Na^+, and the anions BO_3^{3-}, BF_4^- in the reaction system have a guiding effect on the morphologies and particle sizes of CaF_2 particles. Wang *et al.*[24,25] suggested that the cations coming from the different fluoride sources XF (X = K^+, H^+, NH_4^+, Na^+, Rb^+, and Cs^+) are selectively adsorbed on the different crystals facets of nano-particles, resulting in the formation of various shapes. Filankembo *et al.*[26] suggested that the anions Cl^- and Br^- in the added salts are also selectively adsorbed on the different crystal faces of particles to control the morphologies of the products. It is reasonable to assume a similar case for the effects of the cations NH_4^+, Na^+, and the anions BO_3^{3-}, BF_4^- on the morphologies. At the early stages of the reactions, due to the strong interactions between NH_4^+/Na^+ cations and F^- anions, these two cations can be selectively adsorbed on specific facets of the initial CaF_2 particles and change their surface energies. The growth rate of CaF_2 crystal is probably different, owing to the absorption ions NH_4^+ and Na^+ with different radii, which leads to different particle sizes. Furthermore, the cubic CaF_2 seed has an isotropic unit cell structure, which generally induces the isotropic growth of particles and therefore, the NH_4^+ and Na^+ can affect the growth rate in all directions, respectively. Meanwhile, the anions BO_3^{3-} and BF_4^- can destroy chemical bond Ca–EDTA. It can accelerate the release of Ca^{2+} into the solution from the Ca^{2+} chelate complexes. As a result, the non-uniform particles are obtained (as shown in Fig. 2(b)) due to particles growing quickly after nucleation. Figure 2(c) displays the SEM image of CaF_2 particles in the presence of citric acid (CA) and $NaBF_4$ as the fluoride source while other conditions are unchanged. It can be observed that the uniform and cubic CaF_2 nano-particles, whose average size is about 100 nm, are obtained. Under this experimental condition, chelating ligands will firstly mobilize calcium ions at the first step to generate Ca–CA complexes, according to Eqs. (5) and (6). For the formation of CaF_2, we propose the following possible reaction pathways:

$$Ca^{2+} + (Hcit)^{2-} \rightarrow Ca(Hcit)\ (complex), \quad (5)$$

$$Ca^{2+} + 2(H_2cit)^- \rightarrow Ca(H_2cit)_2\ (complex), \quad (6)$$

$$BF_4^- + 3H_2O \rightarrow 3HF + F^- + H_3BO_3, \quad (7)$$

$$Ca(Hcit) + Ca(H_2cit)_2 + 4F^- \rightarrow 2CaF_2 + (Hcit)^{2-} + 2(H_2cit)^-. \quad (8)$$

With the increase of reaction time and temperature, Ca^{2+} ions are released from the complexes mentioned above. Then the F^- anions in the solution react with the free Ca^{2+} to generate CaF_2 nuclei according to Eqs. (7) and (8). With the reaction time ticking by, these nuclei gradually grow into big particles. Comparing the two chelating reagents (Na_2EDTA and CA) in the present work, a large chelate constant ($\lg\beta$) will benefit the stabilization of the complex. The chelate constant is larger for EDTA ($\lg\beta$ = 18–19) than that of citrate acid ($\lg\beta$ = 8–9).[27] So the Ca–CA complex is far less stable than the Ca–EDTA complex. On increasing the reaction temperature to a certain value, large quantities of Ca^{2+} ions are released from Ca–CA complexes, the nucleation and growth of CaF_2 will undergo a short process. But at the same time, the citrate ions dissociated from the Ca–CA complexes are then selectively adsorbed on the surfaces of growing particles, which significantly inhibits their growth.[28,29] Particularly, $(Hcit)^{2-}$ and $(H_2cit)^-$ can inhibit the growth of CaF_2, when the particle size reaches a certain value. Therefore, the CaF_2 particle size is uniform and the adjacent particles can connect with each other. It is possible that the growth by regular aggregation of these stabilized particles proceeds more rapidly than the coarsening of the individual particles. Once being aggregated, these particles are probably held together by electrostatic interaction or van der Waals forces, side by side, to form the larger cubic particles and the rod-like particles. Herein, a schematic diagram of the process is demonstrated in Fig. 2(d).

3.2. Up-conversion photoluminescence and mechanism

As is well known, the CaF_2 is an efficient host lattice for the UC process due to its lower phonon energy.[16] Figure 3 displays the UC spectra of samples obtained under different synthesis conditions. It is clearly observed that the UC spectra of samples exhibit two distinct emission bands peaking at 540 nm and 644 nm, respectively, under the excitation of a 980-nm semiconductor laser. The former intense green emission could be assigned to the transitions of $^5S_2/^5F_4 \rightarrow {}^5I_8$ from Ho^{3+}; the latter weak red emission should be attributed to the $^5F_5 \rightarrow {}^5I_8$ transitions of Ho^{3+}. By comparison with UC spectra

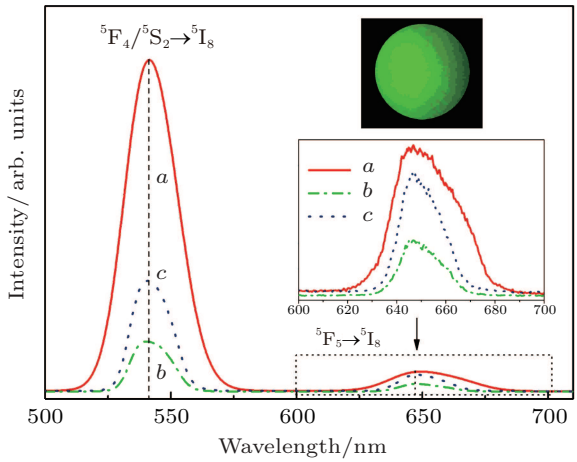


Fig. 3. (color online) UC luminescence spectra of CaF_2:0.5-mol%Ho^{3+}/5-mol%Yb^{3+} samples prepared with different conditions: (curve *a*) NH_4F and Na_2EDTA; (curve *b*) $NaBF_4$ and Na_2EDTA; (curve *c*) $NaBF_4$ and citric acid ($C_6H_8O_7{\cdot}H_2O$). The insets show the photograph of the green light excited at 980 nm and the amplified red emissions in the range 620 nm–680 nm.

of three samples, the UC intensity of the sample prepared with NH_4F and Na_2EDTA is the strongest, and the sample prepared with $NaBF_4$ and Na_2EDTA shows the weakest emission. This result is in agreement with that in Ref. [16], and it is vitally important for enhancing the UC luminescence of the CaF_2 particles with a smaller size. The inset in Fig. 3 shows the amplified red emissions, which show a similar change trend to the green emission band. The sample emits a green light to the naked eye under the excitation of a 980 nm near infrared (NIR) laser diode, and the photograph is shown in the inset of Fig. 3.

The concentration of the dopant has a great effect on the UC luminescence intensity of phosphor, thus a series of samples with different Ho^{3+} or Yb^{3+} concentrations is prepared to determine the optimal compositions of Ho^{3+}/Yb^{3+} co-doped CaF_2, and their room temperature UC luminescent spectra are shown in Fig. 4. Figure 4(a) shows the UC emission spectra of CaF_2: x-mol% Ho^{3+}, y-mol% Yb^{3+} with Ho^{3+} concentrations ranging from $x = 0.3$ mol% to 1.0 mol%, with the Yb^{3+} content fixed at 5 mol%, and in Fig. 4(b), with the Ho^{3+} concentration fixed at 0.5 mol% and Yb^{3+} concentrations y = 2, 5, 10, and 15 under the excitation of a 980 nm laser. All UC spectra are similar to those in Fig. 3 and consist of a strong green emission peaking near 540 nm and a weak red emission peaking around 644 nm, which contribute to the intra 4f–4f transitions of Ho^{3+}. As seen in Fig. 4, it is observed that the UC integrated intensities of green and red emissions (measured as the area under the emission band) become stronger with the increase of Ho^{3+} (activator) or Yb^{3+} (sensitizer) content value, and weaker after having reached a maximum at 0.5 mol% for Ho^{3+} or 10 mol% for Yb^{3+} due to the concentration quenching effect. The concentration quenching effect could be explained by the energy transfer between the nearest dopant ions (activator → activator or sensitizer → activator). From the inset of Fig. 4(a), it is quite clear that the emission intensity increases at the beginning and then decreases due to the concentration quenching effect after having reached the maximum at the Ho^{3+} concentration $x = 0.5$ mol%. The concentration quenching effect caused by the migration of excitation energy from one activator to another lasts until a quenching site is reached and the energy is lost nonradiatively. The concentration quenching effect will not occur at low concentration,

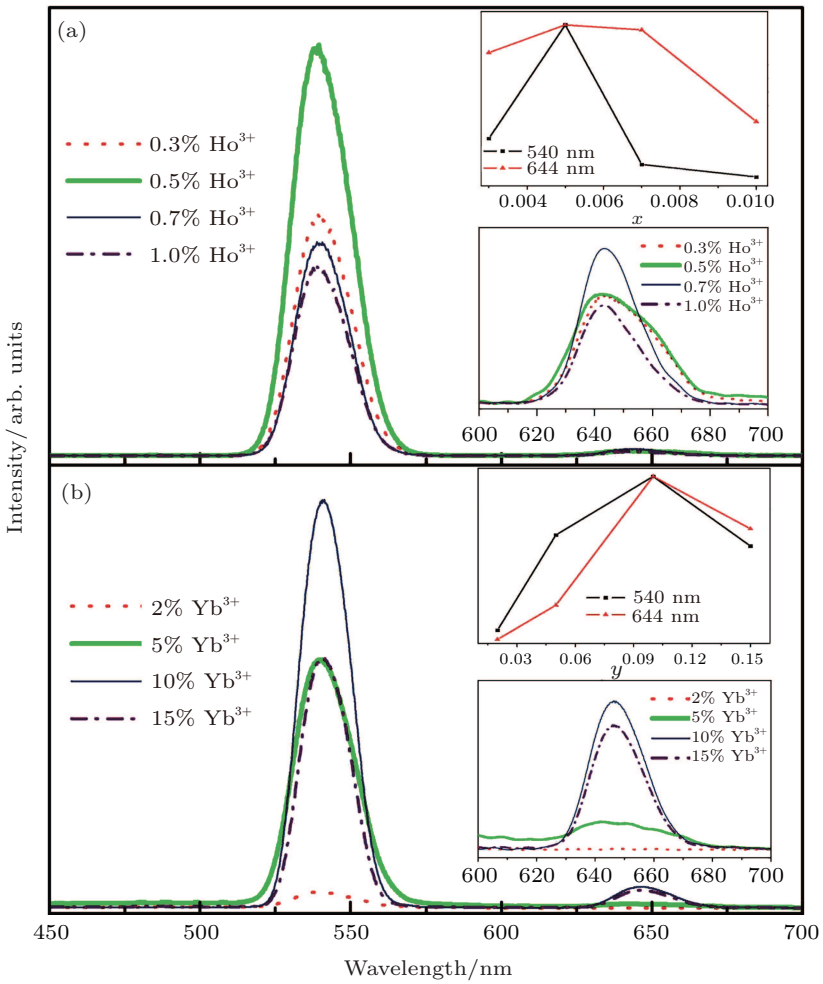


Fig. 4. (color online) UC luminescence spectra of CaF_2: x-mol% Ho^{3+}, y-mol% Yb^{3+} prepared with NH_4F and Na_2EDTA (a) x = 0.3, 0.5, 0.7, and 1.0, y = 5; (b) x = 0.5, y = 2, 5, 10, and 15. Insets show the dependences of normalized UC intensities on Ho^{3+}/Yb^{3+} concentration, and the amplified red region spectra.

because the distance between identical Ho^{3+} ions is so large that the energy migration is hampered.[30] With the increase of the Ho^{3+} concentration, the average distance between Ho^{3+} ions becomes shorter and the energy transfer becomes convenient. As shown in the inset of Fig. 4(b), the UC luminescence intensity becomes stronger with the increase of the Yb^{3+} concentration and reaches a maximum at 10 mol% in the range of 2 mol%–15 mol% with an invariable Ho^{3+} concentration (0.5 mol%). It is generally accepted that an efficient energy transfer takes place from Yb^{3+} to adjacent Ho^{3+}. In the meantime, the back energy transfer from Ho^{3+} to Yb^{3+} also exists. At low concentration, it is the dominant energy transfer from Yb^{3+} to Ho^{3+}. With the increase of the Yb^{3+} content value, the distance between dopant ions will decrease, which promotes back energy transfer and leads to the decrease of UC emission intensity.[31] Therefore, the optimal composition of the UC phosphors is CaF_2:0.5%Ho^{3+}/10%Yb^{3+} with the strongest emission.

Figure 5(a) shows the up-conversion spectra of CaF_2:0.5-mol%Ho^{3+}/10-mol%Yb^{3+} samples prepared with NH_4F and Na_2EDTA each as a function of the pump power under 980-nm NIR excitation. It is found that the UC intensities of samples increase with the pumping power increasing. Generally, the relationship between UC emission intensity (I) and pump power (P) is approximately expressed as follows: $I \propto P^n$, where n is the number of excitation photons absorbed by RE ions at ground states and then transited to the excited states.[32] The power dependence of the up-conversion signal for the product is analyzed using the double logarithmic and the results are depicted in the inset of Fig. 5(a). Here, the photoluminescence intensity I integrated areas of UC spectra ranging from 500 nm–600 nm for green emission and 600 nm–700 nm for red emission are shown. As is well known, the slopes of these curves (n) give the numbers of photons involved in the excitation process for different UC bands. Values of 1.97 and 1.88 are obtained for n corresponding to the 540-nm and 644-nm emission bands, respectively, which indicates that the green and red excited states are predominantly populated by a two-photon absorption process.

Based on the above results and energy matching for pairs of transitions, a possible up-conversion mechanism including energy transfer (ET) in Ho^{3+}/Yb^{3+} co-doped CaF_2 nanoparticles with an excitation of 980-nm is proposed as illuminated in Fig. 5(b). Firstly, the Yb^{3+} is excited from the ground state $^2F_{7/2}$ level to the excited state $^2F_{5/2}$ level under 980-nm pumping, and transfers its energy to Ho^{3+} from the $^2F_{5/2}$ level of Yb^{3+}. Thus, Ho^{3+} is raised from the $^5I_8$ ground state to the $^5I_6$ excited state. This is a phonon-assisted energy transfer process because of the energy mismatch between the $^2F_{5/2}$ level of Yb^{3+} and the $^5I_6$ level of Ho^{3+} (energy gap ΔE is 1549 cm^{-1}).[33] Usually, the phonon-assisted energy transfer process should accompany the compensation for the energy difference. Secondly, $^5S_2$/$^5F_4$ levels of Ho^{3+} can be populated via excited state absorption (ESA) of $^5I_6$ or ET from the Yb^{3+}. Finally, the excited Ho^{3+} ions radiatively relax from the $^5S_2$/$^5F_4$ levels to the ground state, producing strong green emission at about 540 nm. The red emission centered at 644 nm originates from the $^5F_5 \rightarrow {}^5I_8$ transition of Ho^{3+}, and the $^5F_5$ level can be populated through three possible pathways. One pathway is a non-radiative relaxation from $^5S_2$/$^5F_4$ levels to the $^5F_5$ level. Another route is due to the nonradiative decay of intermediate excited state $^5I_6$ to the $^5I_7$ level, from which the populations can be promoted to the higher $^5F_5$ level by ESA or ET from the neighboring Yb^{3+}. Moreover, cross relaxation (CR) can also contribute to the populating of the emitting level $^5F_5$:Ho^{3+}($^5S_2$/$^5F_4$) + Ho^{3+}($^5I_7$) $\rightarrow$ Ho^{3+}($^5F_5$) + Ho^{3+}($^5I_6$).[34] From Fig. 5(a) it follows that the green emission intensity is much more intense than

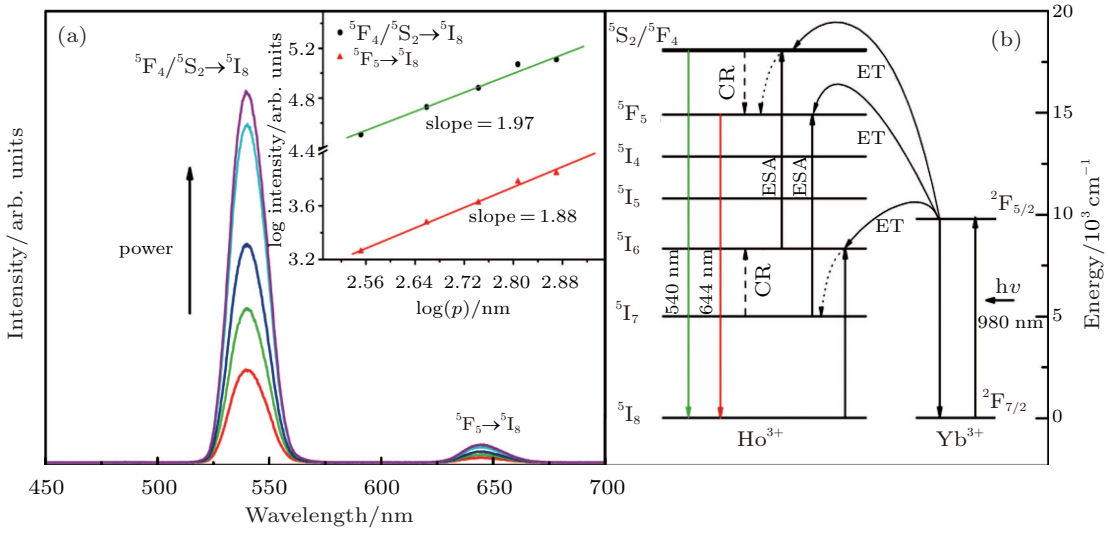


Fig. 5. (color online) (a) Power-dependent UC spectra of CaF_2:0.5-mol%Ho^{3+}/10-mol%Yb^{3+} nano-particles prepared with NH_4F and Na_2EDTA, and (b) schemes of Ho^{3+}, Yb^{3+} ions and energy transfers proposed for UC emission in the sample with 980-nm NIR excitation. Inset shows dependences of the green and red UC on pumping power.

the red emission intensity, which clearly demonstrates that the populations in the $^5I_6$ level, excited to the $^5S_2/^5F_4$ levels, are far more than those decaying nonradiatively to the $^5I_7$ level and the rate of the populations in the $^5S_2/^5F_4$ levels nonradiatively relaxing to the $^5F_5$ level is lower. Lower phonon energy of CaF_2 should respond to this occurrence.

4. Conclusions

In this paper, UC phosphors CaF_2:Ho^{3+}/$Yb^{3+}$are successfully synthesized by a facile hydrothermal approach through using different fluoride sources NH_4F or $NaBF_4$ and different chelating reagents Na_2EDTA or citric acid. Results indicate that cubic phase CaF_2:Ho^{3+}/Yb^{3+} UC phosphors could be obtained and that both the fluoride source and the chelating reagent play key roles in controlling the morphologies and sizes of the particles. Under the excitation of a 980-nm laser, CaF_2:Ho^{3+}/Yb^{3+} nano-particles show a bright green light and its UC spectra include an intense green emission peaking at 540 nm and a weak red emission peaking at 644 nm from the transitions $^5S_2/^5F_4 \rightarrow ^5I_8$ and $^5F_5 \rightarrow ^5I_8$ of Ho^{3+}, respectively. The optimal composition of the present UC phosphors is CaF_2:0.5-mol%Ho^{3+}/10-mol%Yb^{3+}. Moreover, the growth mechanism and the UC mechanism of the present phosphors are also proposed. The present UC phosphor CaF_2:0.5-mol%Ho^{3+}/10-mol%Yb^{3+} could be a promising candidate for applications in biomedicine.

References

[1] Wang M, Liu J L, Zhang Y X, Hou W, Wu X L and Xu S K 2009 *Mater. Lett.* **63** 325
[2] Li C R, Li S F, Dong B, Sun J C, Bo X F and Fan X N 2012 *Chin. Phys. B* **21** 097803
[3] Huang Y and Lieber C M 2004 *Pure Appl. Chem.* **76** 2051
[4] Wang L Y, Yan R X, Huo Z Y, Wang L, Zeng J H, Bao J, Wang X, Peng Q and Li Y D 2005 *Angew. Chem. Int. Ed.* **44** 6054
[5] Jiang T, Qin W P and Zhao D 2012 *Mater. Lett.* **74** 54
[6] Chen X B, Zhang F C and Chen L 2003 *Chin. Phys.* **12** 1451
[7] Cao T Y, Yang T S, Gao Y, Yang Y, Hu H and Li F Y 2010 *Inorg. Chem. Commun.* **13** 392
[8] Wang F, Banerjee D, Liu Y, Chen X and Liu X 2010 *Analyst.* **135** 1839
[9] Cheng L, Yang K, Zhang S, Shao M W, Lee S T and Liu Z 2010 *Nano Res.* **3** 722
[10] Wang Y, Qin W P, Di W H, Zhang J S and Cao C Y 2008 *Chin. Phys. B* **17** 3300
[11] Wang D F, Zhang X D, Liu Y J, Wu C Y, Zhang C S, Wei C C and Zhao Y 2013 *Chin. Phys. B* **22** 027801
[12] Menyuk N, Dwight K and Pierce J 1972 *Appl. Phys. Lett.* **21** 159
[13] Ma D K, Yang D P, Jiang J L, Cai P and Huang S M 2010 *CrystEngComm.* **12** 1650
[14] Jacobsohn L G, Kucera C, James T, Sprinkle K, DiMaio J R, Kokuoz B, Yazgan K B, DeVol T A and Ballato J 2010 *Materials* **3** 2053
[15] Jacob M V, Mazierska J, Ledenyov D and Krupka J 2003 *J. Eur. Ceram. Soc.* **23** 2617
[16] Wang G F, Peng Q and Li Y D 2009 *J. Am. Chem. Soc.* **131** 14200
[17] Lee T H and Heo J 2006 *Phys. Rev. B* **73** 144201
[18] Li L, Guo C F, Chen Y Q, Li T and Jeong J H 2013 *Mater. Lett.* **95** 52
[19] He E J, Liu N, Zhang M L, Qin Y F, Guan B G, Li Y and Guo M L 2012 *Chin. Phys. B* **21** 073201
[20] Shannon R 1976 *Acta Crystallogr. A* **32** 751
[21] Chen J X, Ye S, W X and Qiu J R 2008 *Chin. Phys. Lett.* **25** 2078
[22] Sun Y J, Chen Y, Tian L J, Yu Y, Kong X G, Zhao J W and Zhang H 2007 *Nanotechnology* **18** 275609
[23] Li W J, Shi E W and Fukuda T 2003 *Cryst. Res. Technol.* **38** 847
[24] Wang M, Huang Q L, Hong J M, Chen X T and Xue Z L 2006 *Cryst. Growth Des.* **6** 1972
[25] Wang M, Huang Q L, Hong J M, Chen X T and Xue Z L 2006 *Cryst. Growth Des.* **6** 2169
[26] Filankembo A, Giorgio S, Lisiecki I and Pileni M P 2003 *J. Phys. Chem. B* **107** 7492
[27] Moeller T, Martin D F, Thompson L C, Ferrús R, Feistel G R and Randall W J 1965 *Chem. Rev.* **65** 1
[28] Jiang D L, Li D, Xie J M, Zhu J J, Chen M, Lü X M and Dang S C 2010 *J. Colloid Interface Sci.* **350** 30
[29] Li C X, Quan Z W, Yang P P, Yang J, Lian H Z and Lin J 2008 *J. Mater. Chem.* **18** 1353
[30] Guo C F, Ding X, Seo H J, Ren Z Y and Bai J T 2011 *J. Alloys Compd.* **509** 4871
[31] Chung J H, Ryu J H, Lee S Y, Kang S H and Shim K B 2013 *Ceram. Int.* **39** 1951
[32] Li C R, Dong B, Li L and Lei M K 2008 *Chin. Phys. B* **17** 224
[33] Li X J, Nie Q H, Dai S X, Xu T F, Shen X and Zhang X H 2007 *J. Phys. Chem. Solids* **68** 1566
[34] Tang M M, Wang X S, Peng D F, Wang W, Sun H Q and Yao X 2012 *J. Alloys Compd.* **529** 49